Chandra, R.; Holm, A.; Groth, M.

Impact of vibrationally and electronically excited H_2 on the molecular assisted recombination rate in detached plasma regimes

Published in:
Nuclear Materials and Energy

DOI:
10.1016/j.nme.2022.101360

Published: 01/03/2023

Document Version
Publisher's PDF, also known as Version of record

Nuclear Materials and Energy 34 (2023) 101360

Contents lists available at ScienceDirect

Nuclear Materials and Energy

journal homepage: www.elsevier.com/locate/nme

Impact of vibrationally and electronically excited H_2 on the molecular assisted recombination rate in detached plasma regimes

R. Chandra *, A. Holm, M. Groth

Aalto University, Espoo, Finland

ARTICLE INFO

Keywords:
Divertor
Plasma recombination
Electronic transition
Collisional-radiative

ABSTRACT

The vibrational redistribution of H_2 molecules via the $B^1\Sigma_u^+$ and $C^1\Pi_u$ states are included in the determination of molecular assisted recombination (MAR) rates and are found to have negligible impact in detached plasma regimes. In high recycling and detached divertor plasma conditions, MAR occurs through the higher levels ($v \geq 4$) of vibrationally excited H_2 which are primarily populated through direct electron impact excitation or the electronic excitation of H_2 molecules and the subsequent radiative decay to another vibrational state. We use the collisional-radiative model CRUMPET to evaluate MAR rate coefficients with electronic transitions included, which are applied to detached plasma parameters found in the linear plasma device Magnum-PSI.

1. Introduction

Plasma recombination in the divertor region is considered to be an explanation for the decrease of plasma particle flux to the divertor targets in detached plasma regimes [1]. Plasma recombination occurs mainly from radiative and three-body recombination, which are collectively termed electron-ion recombination (EIR) [2]. EIR becomes relevant only at electron temperatures of 1 eV or below. The presence of molecules contributes to the plasma recombination via molecular assisted recombination (MAR) processes, which are relevant at electron temperature higher than EIR ($1 < T_e < 5$ eV) [1,3]. For hydrogen in divertor plasma conditions, MAR occurs through the higher levels ($v \geq 4$) of vibrationally excited H_2. Hence, the population distribution of the H_2 vibrational states influences plasma recombination through MAR. The vibrational states of H_2 are primarily populated through electron impact excitation of the vibrational number v to a higher number w via two channels [4–6]:

$$H_2(v) + e \rightarrow H_2^- \rightarrow H_2(w) + e \tag{1}$$

$$H_2(v) + e \rightarrow H_2(B^1\Sigma_u^+, C^1\Pi_u) + e \rightarrow H_2(w) + e + h\nu \tag{2}$$

The first reaction is a resonant mechanism involving the temporary formation of H_2^- [6,7]. It is the vibrational excitation process commonly included in vibrationally resolved recombination rate coefficients [8] used in coupled fluid-kinetic edge codes such as SOLPS [9], EDGE2D-EIRENE [10,11], or B2.5-Eunomia [12]. The second reaction excites the vibrational levels indirectly through electronic excitation of the molecule followed by radiative decay [5,6]. To the authors knowledge, the second reaction was not commonly included in the derivation of effective recombination rate coefficients (e.g. AMJUEL [8]) used in fluid-kinetic edge codes.

This paper evaluates the effect of (2) to the vibrational population distribution of H_2 and consequently to the MAR rate for electron densities and temperatures expected in the detached plasma regime of a tokamak. The collisional-radiative model CRUMPET [3] is used to solve the population distribution of the H_2 vibrational states for certain plasma parameters and is explained in Section 2. Using the H_2 vibrational state distribution obtained from CRUMPET, the effective recombination rate coefficients of MAR processes are re-evaluated with (2) included and the results are presented in Section 3. The effect of electronic transitions of H_2 to the particle balance in detached plasma regime is evaluated using data from fluid-kinetic code simulations of plasmas in the linear plasma device Magnum-PSI and is shown in Section 4. We summarize our conclusions in Section 5.

2. CR model species and reactions

The population distribution of $H_2(v)$ (vibrationally excited H_2 in the electronic ground state) is calculated using the collisional-radiative model CRUMPET [3]. CRUMPET allows flexibility in N number of species considered in the equation [13]:

$$\dot{\boldsymbol{n}} = M\boldsymbol{n} + \boldsymbol{\Gamma} \tag{3}$$

where Γ is the source term, $\boldsymbol{n}$ is the density of species considered, and the $N \times N$ rate matrix M. For this paper, the species considered are:

* Corresponding author.
E-mail address: ray.chandra@aalto.fi (R. Chandra).

https://doi.org/10.1016/j.nme.2022.101360
Received 23 June 2022; Received in revised form 20 December 2022; Accepted 28 December 2022
Available online 2 January 2023

Table 1
List of collisional processes included in the rate matrix M in CRUMPET. For H2VIBR, i refers to the vibrational mode number.

Nr.	Reaction formula	Data ref.
1	$H_2(v) + e \rightarrow H_2^- \rightarrow H_2(v \pm 1) + e$	H2VIBR 2.iv($i+1$) [15–17]
2	$H_2(v) + e \rightarrow H_2(B^1\Sigma_u^+, v') + e$	MCCC [18]
3	$H_2(v) + e \rightarrow H_2(C^1\Pi_u, v') + e$	MCCC [18]
4	$H_2(B^1\Sigma_u^+, v') \rightarrow H_2(w) + h\nu$	[19]
5	$H_2(C^1\Pi_u, v') \rightarrow H_2(w) + h\nu$	[19]
6	$H_2(v) + e \rightarrow e + H + H$	H2VIBR 2.il1 [15,17][a]
7	$H_2(v) + H^+ \rightarrow H_2^+ + H$	H2VIBR 2.il2 [15,17,20][a]
8	$H_2(v) + e \rightarrow H^- + H$	H2VIBR 2.il3 [7,15,17][a]

[a]The reader is recommended to revisit the H2VIBR dataset as it may be outdated.

1. 15 vibrational levels of the electronic ground state of H_2, $H_2(X^1\Sigma_g^+)(v), v = 0 - 14$
2. 37 vibrational levels of the first electronically excited singlet state of H_2, $H_2(B^1\Sigma_u^+)(v), v = 0 - 36$
3. 14 vibrational levels of the second electronically excited singlet state of H_2, $H_2(C^1\Pi_u)(v), v = 0 - 13$
4. the molecular ion H_2^+
5. the negative ion H^-
6. the electronic ground state of H

The applicability of CRUMPET is only limited by the availability of reaction rate coefficients necessary to construct M [3]. The collisional processes included in M and the available cross-section or rate coefficient data are summarized in Table 1. Direct electron impact vibrational excitation (1) is treated as ladder-like, where only single step transitions are allowed. For electronic excitation of H_2 (2 and 3 in Table 1), all possible transitions between vibrational levels are included. The same applies for optical transitions (4 and 5 in Table 1). The $H_2(v)$ population can be depleted through dissociation, ion conversion (IC), and the dissociative attachment (DA) process (6,7 and 8 in Table 1). The reaction rates are calculated assuming $T_e = T_i$. The direct ionization of H_2 is not included in CRUMPET for the purpose of comparison with simulation data [14] later in Section 4, which also does not include this process. It is advised to include direct ionization in the future, especially when the electron temperature can exceed 4 eV, where it starts to compete with ion conversion and dissociation.

Two different CRUMPET inputs are created to demonstrate the effect of electronic transitions to the population distribution of $H_2(v)$. The first input considers only the electronic ground state of H_2, H_2^+. H^-, and H. The second input considers the electronically excited states of H_2 in addition to all off the species of the first input. Hence, the rate matrix M have the size 18 × 18 and 69 × 69 for the first and second input respectively. The first input will be referred to as no electronic (no el.) in the figures presented in the paper.

3. Effect of H_2 electronic transitions to MAR rate

With increasing T_e, the population distribution is shifted towards higher vibrational states of H_2 when the electronic transitions of H_2 are included in the model. This trend is reversed when electronic transitions are not included, as shown by the population distributions of $H_2(v)$ for electron temperatures $T_e = 1, 3,$ and 5 eV in Fig. 1. Indeed, the reaction rates for the electronic transition to the singlet B and C states, as described in reaction number 2 and 3 in Table 1, are expected to be dominant for higher electron impact energies [4].

The shift towards higher vibrational population states can potentially increase the effective recombination rate through the MAR process, both through the IC and the DA channel. The effective rate coefficient for these two channels can be calculated as follows:

$$\langle \sigma v \rangle_{eff} = \sum_{v=0}^{14} \langle \sigma v \rangle_v \; P_{H_2(v)} \tag{4}$$

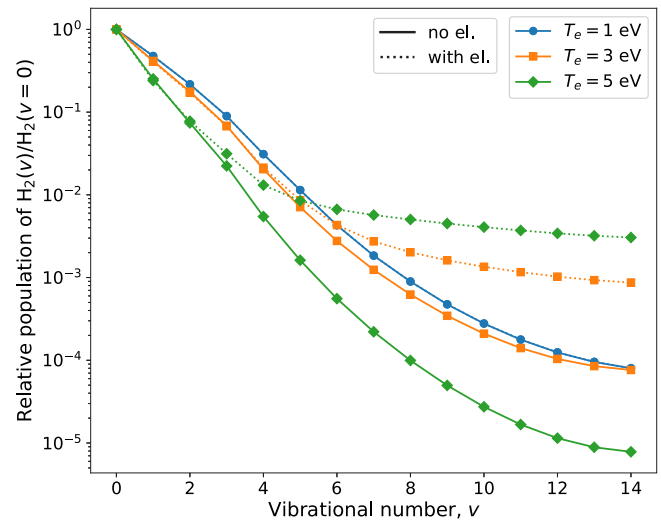

Fig. 1. Population of $H_2(v)$ relative to the ground vibrational state $H_2(v = 0)$. The solid line indicates the population distribution when electronic states of H_2 is not considered. The dotted line indicates the population distribution when electronic states are considered. When the re-distribution of $H_2(v)$ via electronic states is included, the distribution is shifted towards higher states with increasing T_e. The rate coefficients are calculated for $n_e = 10^{20}$ m^{-3}.

Table 2
List of subsequent processes causing the annihilation of ions H_2^+ and H^-. Only MAR processes result in plasma recombination. The other pathways are molecular assisted ionization (MAI) and molecular assisted dissociation (MAD) [21,22].

Nr.	Reaction formula		Name	Data ref.
1	$H_2^+ + e \rightarrow$	$2e + H^+ + H^+$	MAI	AMJUEL 2.2.11 [8]
2		$e + H + H^+$	MAD-IC	AMJUEL 2.2.12 [8]
3		$H + H$	MAR-IC	AMJUEL 2.2.14 [8]
4	$H^+ + H^- \rightarrow$	$H + H^+ + e$	MAD-DA	AMJUEL 7.2.3b [8]
5		$H + H$	MAR-DA	AMJUEL 7.2.3a [8]

where $P_{H_2(v)} = H_2(v)/H_2(v = 0)$ is the relative population fraction of $H_2(v)$. The IC and DA processes do not necessarily result in plasma recombination and depend on the subsequent reaction of the ionic products, H_2^+ for IC or H^- for DA. These subsequent reactions are summarized in Table 2. Taking into account these follow-up reactions, a factor can be added to Eq. (4) such that an effective MAR rate can be defined as:

$$\langle \sigma v \rangle_{MAR} = \left(\sum_{v=0}^{14} \langle \sigma v \rangle_v \; P_{H_2(v)} \right) \frac{\langle \sigma v \rangle_{rec}}{\langle \sigma v \rangle_{tot}} \tag{5}$$

where $\frac{\langle \sigma v \rangle_{rec}}{\langle \sigma v \rangle_{tot}}$ is the ratio between rate coefficients of reactions resulting in recombination and the total rate coefficients of all possible reaction depleting the ionic products H_2^+ or H^-. The effective MAR rate coefficients through the IC and DA channel are evaluated for 1000 T_e values evenly spaced in the logarithmic scale between 0.1–1000 eV (Fig. 2). By including the electronic transitions of H_2, the change in the population of the higher vibrational states of $H_2(v)$ alters the effective recombination rate coefficients starting from $T_e = 3$ eV. For the ion conversion channel (MAR-IC), the rate coefficient is enhanced by a factor of 3 at around $T_e = 5$ eV, and by more than an order of magnitude at around $T_e = 15$ eV. The impact of including the electronic transitions of H_2 is even more profound for effective recombination via the dissociative attachment channel (MAR-DA). This pathway becomes a relevant contributor of plasma recombination for $T_e \geq 2$ eV, contrary to when no electronic transitions of H_2 is considered. Furthermore, the rate coefficient is larger by 2 orders of magnitude at around $T_e = 10$ eV.

The electronic transitions of H_2 starts to improve the MAR rates for T_e above 2–3 eV. However, in this temperature range, direct dissociation and ionization deplete the electronic ground state of H_2 as

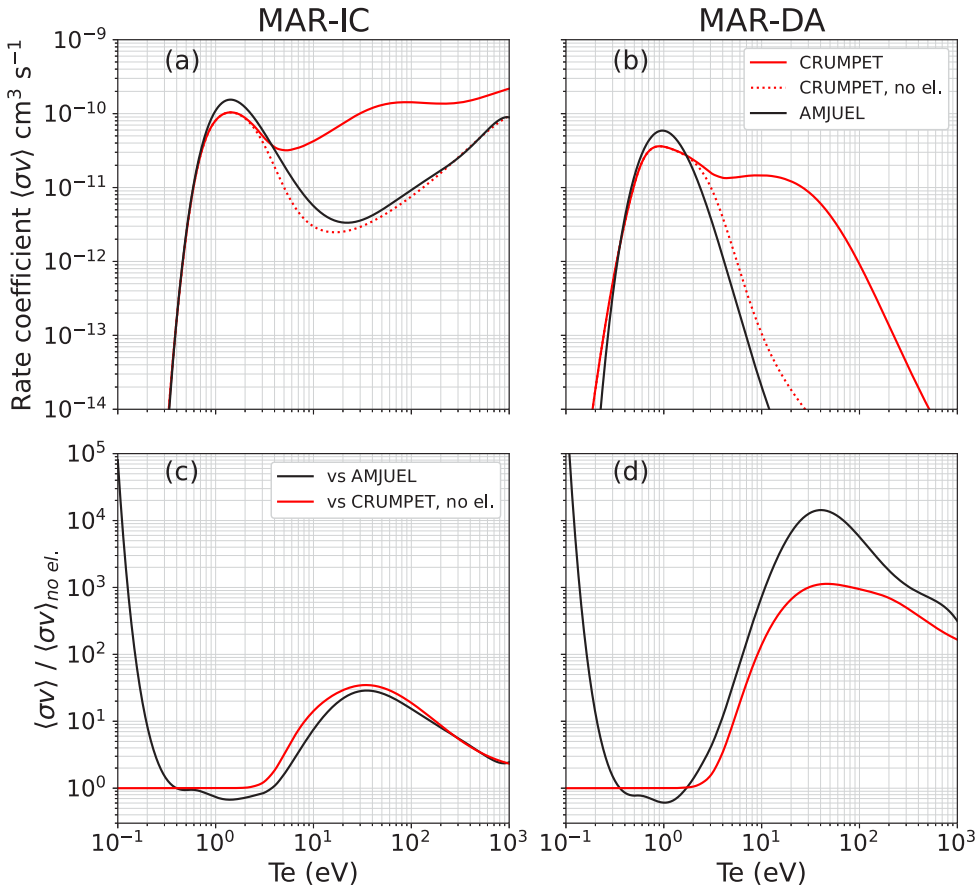

Fig. 2. Effective MAR rate coefficients via ion conversion (MAR-IC) (a) and via dissociative attachment (MAR-DA) (b) pathways calculated with CRUMPET. The rate coefficients are evaluated when the electronic transitions of H_2 are included (red solid line) and neglected (red dotted line). As a comparison, the effective MAR rates from AMJUEL, where electronic transitions are neglected, is shown in black. The relative difference between the CRUMPET rate coefficient and the no el. rate coefficients of AMJUEL (black) and CRUMPET (red) are shown for MAR-IC (c) and MAR-DA (d). The rate coefficients are calculated for $n_e = 10^{20}$ m^{-3}. The AMJUEL rate coefficient collapse faster than CRUMPET at very low temperatures which resulted in the very high ratio numbers shown in (c) and (d). (For interpretation of the references to colour in this figure legend, the reader is referred to the web version of this article.)

a MAR precursor [1]. Direct dissociation and ionization of H_2 are still dominant for T_e above 2 eV even when electronic transitions can significantly enhance MAR rates as shown in Fig. 3. Hence, evaluating the overall impact of electronic transitions of H_2 to the global particle balance requires information on the H_2 ground state density which is coupled with the electron density and temperature.

4. Evaluation of MAR rate in detached plasma regimes

SOL plasma codes, such as SOLPS, EDGE2D-EIRENE, and B2.5-Eunomia, solve the Braginskii equations for the plasma species, and the Boltzmann equation for the neutral species using Monte Carlo methods. They provide self-consistent information of the plasma density, temperature, and neutral densities. A detachment study using B2.5-Eunomia [14] was recently conducted in the linear plasma device Magnum-PSI [23]. Plasma detachment is achieved by increasing the H_2 gas pressure exclusively in a chamber housing the target of the plasma beam using gas puffing [24]. The plasma was observed to be in a varying state of detachment depending on H_2 pressure that is applied within the chamber [24]. We use the plasma density, temperature, and the H_2 density in the electronic and vibrational ground state from B2.5-Eunomia simulations of the several detached plasma states for H_2 pressures of 0.27–2 Pa. The plasma density, temperature, and the H_2 density associated with the different H_2 pressure values are illustrated in Fig. 4. These plasma conditions cover the temperature range where the effect of electronic transitions of H_2 to the effective recombination rate becomes noticeable ($T_e \geq 2$ eV), based on the analysis on the effective MAR rate coefficients in Section 3.

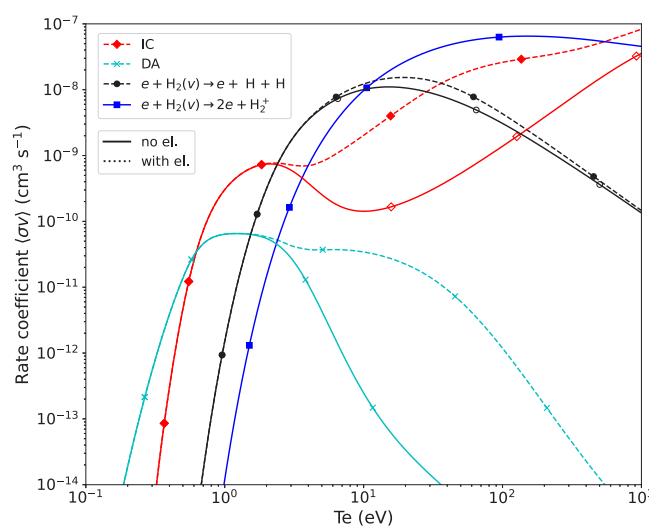

Fig. 3. The rate coefficients of processes that deplete the electronic ground state of H_2. The MAR precursors (IC and DA) compete with direct dissociation (black circle) and ionization (blue square) for $T_e \geq 2$ eV even when the electronic transitions of H_2 are included. The rate coefficients are calculated for $n_e = 10^{20}$ m^{-3}. There is no ionization rate with electronic transitions as it is not included in CRUMPET.

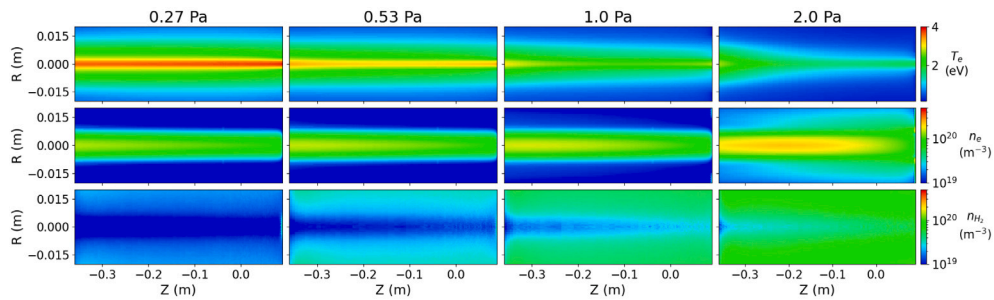

Fig. 4. T_e, n_e and n_{H_2} distributions of the Magnum-PSI plasma beam within the target chamber. The values are obtained from B2.5-Eunomia simulations of varying H_2 pressures of 0.27, 0.53, 1.0 and 2.0 Pa [14], measured near the pumping surface far from the plasma (R = 0.2 m). The target plate is located at the east boundary (Z = 0.09 m).

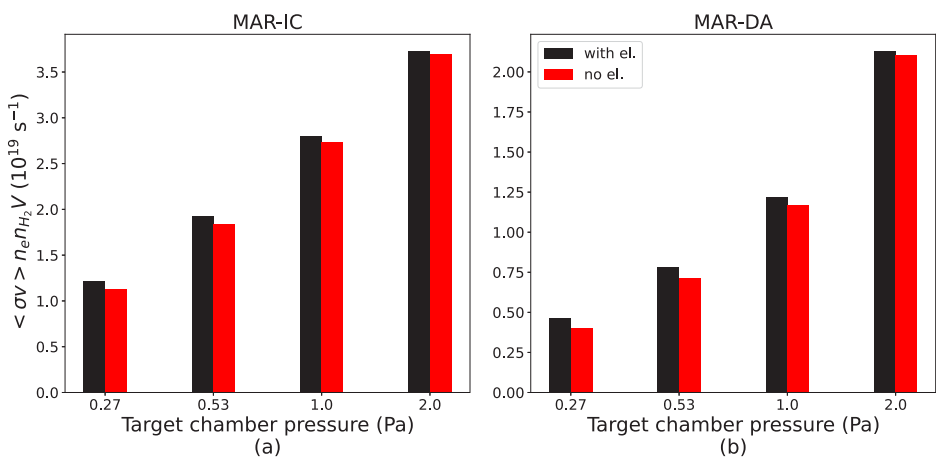

Fig. 5. Global MAR-IC (a) and MAR-DA (b) rates calculated using data shown in Fig. 4. The rates are shown for each simulated pressure level representing the varying stages of plasma detachment. The rate uses $\langle \sigma v \rangle_{MAR}$ with electronic transitions of H_2 included (black) and neglected (red). The impact of electronic transitions of H_2 to the MAR rate is negligible in the detached regime. (For interpretation of the references to colour in this figure legend, the reader is referred to the web version of this article.)

The plasma density, temperature, and the H_2 density in the electronic and vibrational ground state from B2.5-Eunomia are used to calculate the effective recombination rate S_{rec} following (5):

$$S_{rec} = \sum_c \left[\langle \sigma v \rangle_{MAR} \, n_e n_{H_2(v=0)} \, V \right]_c \tag{6}$$

where n_e is the electron density, $n_{H_2(v=0)}$ is the hydrogen molecule density in the electronic and vibrational ground state, V is the plasma volume, and c indicates the quantities to be local in a grid cell of the finite-volume B2.5 code. The grid cells are limited to the plasma region inside the target chamber of Magnum-PSI. The global recombination rate from MAR-IC and MAR-DA pathways for each level of pressures are shown in Fig. 5. By including electronic transitions of H_2 the MAR rates are enhanced marginally in the 'attached' plasma regime for which T_e is around 3–4 eV. The MAR-IC pathway is enhanced by approximately 7% while the MAR-DA pathway shows a larger increase of around 16%. The impact diminishes towards detached plasma regime and becomes negligible at the highest pressure for MAR-IC and MAR-DA, at 0.7% and 2%, respectively.

The same analyses are repeated for the MAD pathways (nr. 2 and 4 in Table 2). While these processes does not produce plasma recombination, they can remove electron energy from the plasma. The electron cooling rate can therefore be higher when electronic transitions are included. Indeed, this increase is readily observed from the increase of global MAD-IC and MAD-DA rates shown in Fig. 6. The MAD-IC and MAD-DA pathways are increased by, respectively, 18% and 59% in the attached plasma regime. Similar with MAR, the impact diminishes towards detached plasma regime to around, respectively, 1% and 3%. However, MAD is expected to be relevant at attached plasma temperatures, and so the electronic transitions should be included in determining MAD rates.

5. Conclusions

The impact of electronic transitions to the singlet B and C states of H_2 on the MAR rate is evaluated using the CR model CRUMPET and data of electron density, temperature and H_2 density from B2.5-Eunomia simulations of plasma detachment in the linear plasma device Magnum-PSI. The impact is highest in the attached plasma regime where the electron temperature is around 3–4 eV, as expected from the modified effective MAR rate coefficients shown in Fig. 2. However, the enhancement diminishes for further plasma detachment, and so remains insufficient to change the system significantly. On the other hand, MAD rates is enhanced substantially in the attached plasma regime where it is relevant, and thus can have major impact in the plasma energy balance. The additional electron cooling may affect plasma recombination indirectly by driving the temperature further down. While this paper uses simulation data from a linear plasma device, these effects are expected to occur in tokamak divertors with similar plasma and neutral conditions, as the effect is dependent mainly on the plasma density, temperature and neutral densities. It is important to note that reactor divertors are subject to other physics such as drifts and complex magnetic geometries which are absent ina linear plasma device. The same approach presented in this paper is readily available for tokamak simulations performed using SOLPS, EDGE2D-EIRENE or other codes, which included the aforementioned physics. These studies should provide more insight in the effect of electronic transitions of H_2 to plasma recombination, and consequently, their effects on plasma detachment.

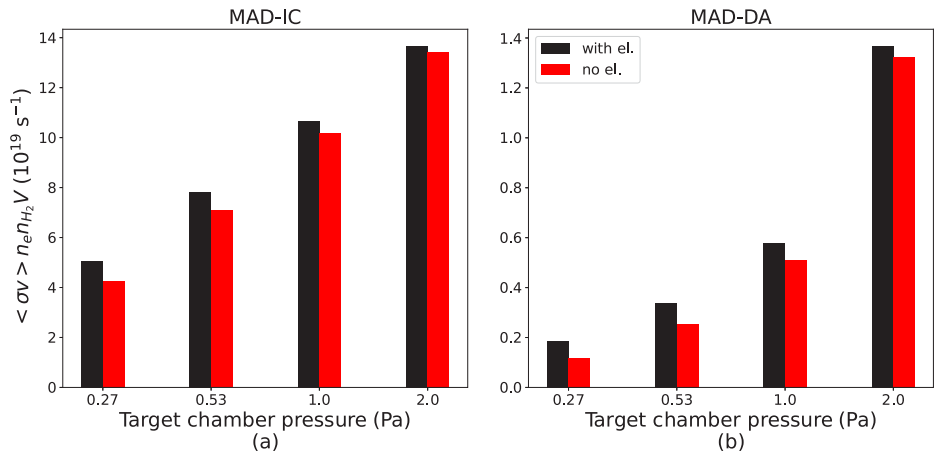

Fig. 6. Global MAD-IC (a) and MAD-DA (b) rates calculated using data shown in Fig. 4. The rates are shown for each simulated pressure level representing the varying stages of plasma detachment. The rate uses $\langle \sigma v \rangle_{MAR}$ with electronic transitions of H_2 included (black) and neglected (red). The MAD pathway does not result in plasma recombination and only removes electron energy from the plasma. The influence of electronic transition to this process can be significant at attached plasma regimes. (For interpretation of the references to colour in this figure legend, the reader is referred to the web version of this article.)

CRediT authorship contribution statement

R. Chandra: Conceptualization, Methodology, Software, Validation, Formal analysis, Data curation, Writing – original draft, Writing – review & editing, Visualization. **A. Holm:** Methodology, Software, Validation, Supervision, Writing – review & editing. **M. Groth:** Writing – review & editing, Supervision, Project administration, Resources, Funding acquisition.

Declaration of competing interest

The authors declare that they have no known competing financial interests or personal relationships that could have appeared to influence the work reported in this paper.

Data availability

Data will be made available on request.

Acknowledgements

This work was supported by the Academy of Finland under grant no. 13330050.

References

[1] S. Krasheninnikov, A. Pigarov, D. Sigmar, Plasma recombination and divertor detachment, Phys. Lett. A 214 (5) (1996) 285–291, http://dx.doi.org/10.1016/0375-9601(96)00185-5.

[2] S.I. Krasheninnikov, A.S. Kukushkin, Physics of ultimate detachment of a tokamak divertor plasma, J. Plasma Phys. 83 (5) (2017) 155830501, http://dx.doi.org/10.1017/S0022377817000654.

[3] A. Holm, P. Börner, T. Rognlien, W. Meyer, M. Groth, Comparison of a collisional-radiative fluid model of H2 in UEDGE to the kinetic neutral code EIRENE, Nucl. Mater. Energy 27 (2021) 100982, http://dx.doi.org/10.1016/j.nme.2021.100982.

[4] K. Sawada, T. Fujimoto, Effective ionization and dissociation rate coefficients of molecular hydrogen in plasma, J. Appl. Phys. 78 (5) (1995) 2913–2924, http://dx.doi.org/10.1063/1.360037.

[5] J.R. Hiskes, Cross sections for the vibrational excitation of the H2(X1 Σ+g) state via electron collisional excitation of the higher singlet states, J. Appl. Phys. 51 (9) (1980) 4592–4594, http://dx.doi.org/10.1063/1.328352.

[6] C. Gorse, M. Capitelli, J. Bretagne, M. Bacal, Vibrational excitation and negative-ion production in magnetic multicusp hydrogen discharges, Chem. Phys. 93 (1) (1985) 1–12, http://dx.doi.org/10.1016/0301-0104(85)85044-8.

[7] J.N. Bardsley, J.M. Wadehra, Dissociative attachment and vibrational excitation in low-energy collisions of electrons with H_2 and D_2, Phys. Rev. A 20 (1979) 1398–1405, http://dx.doi.org/10.1103/PhysRevA.20.1398.

[8] D. Reiter, et al., The data file AMJUEL: Additional atomic and molecular data for EIRENE, in: Electronic File, FZ JÜLich, 2000.

[9] X. Bonnin, W. Dekeyser, R. Pitts, D. Coster, S. Voskoboynikov, S. Wiesen, Presentation of the new SOLPS-ITER code package for tokamak plasma edge modelling, Plasma Fusion Res. 11 (2016) 1403102.

[10] R. Simonini, G. Corrigan, G. Radford, J. Spence, A. Taroni, Models and numerics in the multi-fluid 2-D edge plasma code EDGE2D/U, Contrib. Plasma Phys. 34 (2–3) (1994) 368–373, http://dx.doi.org/10.1002/ctpp.2150340242.

[11] D. Reiter, Progress in two-dimensional plasma edge modelling, J. Nucl. Mater. 196–198 (1992) 80–89, http://dx.doi.org/10.1016/S0022-3115(06)80014-0, Plasma-Surface Interactions in Controlled Fusion Devices.

[12] R.C. Wieggers, D.P. Coster, P.W.C. Groen, H.J. de Blank, W.J. Goedheer, B2.5-Eunomia simulations of Pilot-PSI plasmas, J. Nucl. Mater. 438 (2013) S643 – S646.

[13] P.T. Greenland, Collisional-radiative models with molecules, Proc. R. Soc. Lond. Ser. A Math. Phys. Eng. Sci. 457 (2012) (2001) 1821–1839, http://dx.doi.org/10.1098/rspa.2001.0788.

[14] R. Chandra, H.J. de Blank, P. Diomede, H.J.N. van Eck, H.J. van der Meiden, T.W. Morgan, J.W.M. Vernimmen, E. Westerhof, B2.5-Eunomia simulations of Magnum-PSI detachment experiments: I. Quantitative comparisons with experimental measurements, Plasma Phys. Control. Fusion 63 (9) (2021) 095006, http://dx.doi.org/10.1088/1361-6587/ac11b6.

[15] D. Reiter, The Data File H2VIBR: Additional Molecular Data for EIRENE: Vibrationally Resolved H2 (X) Ground State, Forschungszentrum Juelich GmbH, 2005.

[16] W.T. Miles, R. Thompson, A.E.S. Green, Electron-impact cross sections and energy deposition in molecular hydrogen, J. Appl. Phys. 43 (2) (1972) 678–686, http://dx.doi.org/10.1063/1.1661176.

[17] R.K. Janev, W.D. Langer, E. Douglass Jr., et al., Elementary Processes in Hydrogen-Helium Plasmas: Cross Sections and Reaction Rate Coefficients, Springer Science & Business Media, 2012, http://dx.doi.org/10.1007/978-3-642-71935-6.

[18] L.H. Scarlett, D.V. Fursa, M.C. Zammit, I. Bray, Y. Ralchenko, K.D. Davie, Complete collision data set for electrons scattering on molecular hydrogen and its isotopologues: I. Fully vibrationally-resolved electronic excitation of H2(X1 Σg+), At. Data Nucl. Data Tables 137 (2021) 101361, http://dx.doi.org/10.1016/j.adt.2020.101361.

[19] U. Fantz, D. Wünderlich, Franck–Condon factors, transition probabilities, and radiative lifetimes for hydrogen molecules and their isotopomeres, At. Data Nucl. Data Tables 92 (6) (2006) 853–973, http://dx.doi.org/10.1016/j.adt.2006.05.001.

[20] M.G. Holliday, J.T. Muckerman, L. Friedman, Isotopic studies of the proton–hydrogen molecule reaction, J. Chem. Phys. 54 (3) (1971) 1058–1072, http://dx.doi.org/10.1063/1.1674939.

[21] U. Fantz, D. Reiter, B. Heger, D. Coster, Hydrogen molecules in the divertor of ASDEX Upgrade, J. Nucl. Mater. 290–293 (2001) 367–373, http://dx.doi.org/10.1016/S0022-3115(00)00638-3, 14th Int. Conf. on Plasma-Surface Interactions in Controlled Fusion D evices.

[22] S.I. Krasheninnikov, A.S. Kukushkin, A.A. Pshenov, Divertor plasma detachment, Phys. Plasmas 23 (5) (2016) 055602, http://dx.doi.org/10.1063/1.4948273.

[23] H. van Eck, G. Akkermans, S. Alonso van der Westen, D. Aussems, M. van Berkel, S. Brons, I. Classen, H. van der Meiden, T. Morgan, M. van de Pol, J. Scholten, J. Vernimmen, E. Vos, M. de Baar, High-fluence and high-flux performance characteristics of the superconducting Magnum-PSI linear plasma facility, Fusion Eng. Des. 142 (2019) 26–32, http://dx.doi.org/10.1016/j.fusengdes.2019.04.020.

[24] R. Perillo, G. Akkermans, I. Classen, W. Vijvers, R. Chandra, K. Jesko, S. Korving, J. Vernimmen, M. de Baar, Experimental evidence of enhanced recombination of a hydrogen plasma induced by nitrogen seeding in linear device Magnum-PSI, Nucl. Mater. Energy 19 (2019) 87–93, http://dx.doi.org/10.1016/j.nme.2019.02.018.